基于反射峰面积的水体叶绿素遥感反演模拟研究

马万栋[1],王 桥[1],吴传庆[1],殷守敬[1],邢前国[2],朱 利[1],吴 迪[1]

(1. 环境保护部卫星环境应用中心,北京 100094;2. 中国科学院烟台海岸带研究所,烟台 264003)

摘要:叶绿素浓度是水体富营养化状态的重要指标,也是水色遥感反演的水质参数之一。水体中叶绿素浓度的遥感反演主要是建立实测光谱和实测水质参数二者之间的关系模型,利用遥感影像进行叶绿素浓度的信息提取。传统的叶绿素浓度遥感反演受区域性和季节性的影响,反演精度不高,而且反演模型不具普适性,需对叶绿素光谱特征进行分析,建立高精度的反演模型。本文采用Hydrolight数据模拟了不同叶绿素浓度(1~200 μg·L^{-1})的水体在可见光近红外的反射波谱曲线,通过分析叶绿素的光谱特征选取了特征波段或波段组合,并建立了叶绿素浓度反演模型。研究表明,除反射峰波长模型外,反射峰面积模型、三波段模型、红光线高度模型等均能较好地反演叶绿素浓度。在不同叶绿素反演模型中,除红光线模型外,最优的是反射峰面积模型,其决定系数为0.9689,反演误差为25.25 μg·L^{-1};其次是三波段模型,其决定系数为0.9637,反演误差为10.66 μg·L^{-1}。究其原因,三波段模型考虑了水体中非色素悬浮物、黄色物质及水体后向散射对叶绿素浓度反演造成的影响;反射峰面积模型除此之外还综合考虑了叶绿素散射效率的影响。

关键词:叶绿素;遥感反演;反射峰面积模型;三波段模型

DOI:10.3724/SP.J.1047.2014.00965

1 前言

水体中叶绿素浓度是二类水体水色遥感反演的重要指标之一。叶绿素浓度的遥感反演受不同水色组分光学特性的影响。利用浮游植物在蓝波段的强吸收和绿波段的强反射特征,水体叶绿素遥感反演常利用二波段的比值算法[1-2],但是算法反演精度较低[3-5]。水体叶绿素浓度的遥感反演主要利用其在680 nm左右的反射特性[6-7],如Rrs_{705}/Rrs_{670}及Rrs_{725}/Rrs_{675}等算法、荧光算法等[8]。Stumpf and Tyler[9]研究表明,AVHRR和CZCS的近红外/红波段比值算法能有效地提取藻华,而且对悬浮物浓度大于10 μg·L^{-1}的水体中叶绿素浓度进行了反演。Gons等[10]利用704 nm和672 nm处的反射率及固有光学特性进行了叶绿素浓度的反演。Ruddick等[11]利用比值算法发现近红外波长的位置是影响叶绿素反演精度的主要因素。Dall'Olmo等利用三波段模型反演叶绿素浓度取得了较好的反演结果[4]。三波段模型起源于植被色素含量的算法反演[12-13],后来被推广到悬浮物含量较高水体中叶绿素浓度的反演[5,14-15]。Chen等利用改进的三波段模型对佛罗里达西海岸水体叶绿素进行了反演,有效地去除了黄色物质和悬浮颗粒物的影响,得到了较高的反演精度[16]。马万栋等利用Hydrolight模拟了叶绿素在红波段的光谱反射特征,发现叶绿素的红波段反射峰特征不同于荧光峰[17]。在叶绿素浓度遥感反演中,常使用叶绿素在红波段的反射峰特征选取特征波段或组合,进行数学拟合,实现叶绿素浓度反演[17]。本文通过Hydrolight数据计算了不同组分水体,在可见光和近红外波段的光谱反射率,研究了叶绿素反演的不同方法。

2 数据获取和处理

水体中叶绿素、黄色物质及悬浮物是影响水体颜色的主要组分,也是水体遥感反演的主要水质参数。水体参数浓度的遥感反演取决于叶绿素、黄色物质及悬浮物的固有和表观光学属性。遥感反射率(R_{rs})与吸收系数(a)和后向散射系数(b_b)之间的关系[18-20]可表示为:

收稿日期:2013-10-29;**修回日期**:2014-01-21.

基金项目:水专项课题(2014ZX07508001);国家自然科学基金项目(41271349);环保公益项目(201409100)。

作者简介:马万栋(1977-),男,山东陵县人,博士,主要从事水环境遥感方面研究。E-mail:mawdcn@sohu.com

$$R_{rs}(\lambda)=f\frac{b_b(\lambda)}{a(\lambda)+b_b(\lambda)} \quad (1)$$

式(1)中，λ 是波长；f 是基于水体的表观光学特性而变化的参数；$b_b(\lambda)$ 是水体的总后向散射系数；$a(\lambda)$ 是水体的总吸收系数，包括叶绿素(a_{chla})、悬浮物($a_{tripton}$)、黄色物质(a_{CDOM})及纯水(a_{water})的吸收[21]，可表示为：

$$a(\lambda)=a_{chla}+a_{tripton}+a_{CDOM}+a_{water} \quad (2)$$

利用Hydrolight获取了黄色物质浓度为2 m^{-1}(在440 nm处的吸收系数)、悬浮物浓度为1 mg·L^{-1}、叶绿素浓度为1 μg·L^{-1}的水体，在不同波长的吸收和后向散射，依据辐射传输模型[22-23]、Gordon模型[18]及水气界面的光场分布函数[24-25]，通过计算获取了叶绿素浓度为1~200 μg·L^{-1}的水体在可见光波段的遥感反射率(图1)。

3 水体叶绿素浓度的遥感反演

3.1 反射峰面积模型

本文通过叶绿素在红波段的光谱反射率曲线，选取叶绿素荧光反射峰(Rrs_{max})相邻的两个吸收谷(Rrs_{674}和Rrs_{740})计算叶绿素在红波段的反射峰面积(Normalized Peak Area, NPA)(图2)[26]。

根据反射峰面积示意图，计算叶绿素在红波段的反射峰面积。

$$NPA=\int_{674}^{740}Rrs_{\lambda}\mathrm{d}\lambda-\frac{(Rrs_{674}+Rrs_{740})\times(740-674)}{2} \quad (3)$$

式(3)中，NPA 是叶绿素反射峰面积；Rrs_{λ} 是叶绿素在波长 λ 处的遥感反射率。

依据式(3)分别计算不同叶绿素浓度的反射峰面积NPA。通过研究不同叶绿素浓度与反射峰面积的关系表明，叶绿素浓度和反射峰面积有较好的相关关系(图3)，其决定系数为0.9689，利用该模型对叶绿素浓度进行了反演，其RMS误差为25.25 μg·L^{-1}。

3.2 三波段模型

三波段模型可用式(4)表示：

$$C_{Chla}\propto\left[\frac{1}{R(\lambda_1)}-\frac{1}{R(\lambda_2)}\right]\times R(\lambda_3) \quad (4)$$

式(4)中，C_{Chla} 是叶绿素浓度；$R(\lambda_1)$、$R(\lambda_2)$、$R(\lambda_3)$ 分别表示波长 λ_1、λ_2、λ_3 处的遥感反射率。依据三波段模型的原理，选取λ_1=674 nm、λ_2= 700 nm、λ_3=740 nm建立三波段模型。通过研究发现叶绿素浓度与三波段模型有较好的线性相关关系，其决定系数为0.9637，表达式为：

$$C_{Chla}=198.21\times\left[\frac{Rrs_{740}}{Rrs_{674}}-\frac{Rrs_{740}}{Rrs_{700}}\right]+6.8887 \quad (5)$$

式(5)中，C_{Chla} 是叶绿素浓度。利用该模型对叶绿素浓度进行了反演，其RMS误差为10.66 μg·L^{-1}。

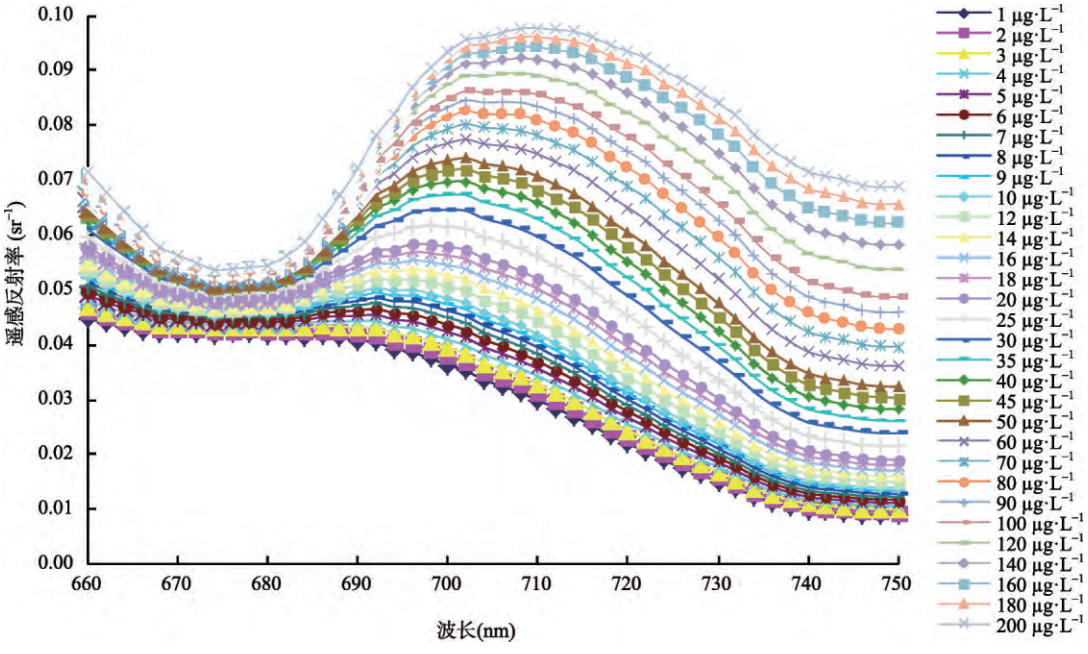

图1 不同叶绿素浓度的水体在红波段的反射率变化曲线

Fig.1 Reflection curves of chlorophyll-a with different concentrations in red band region

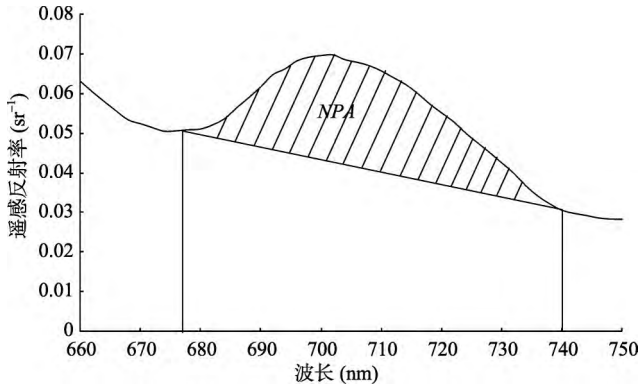

图2　叶绿素红波段反射峰面积示意图

Fig.2　Illustration of the *NPA* in red band region

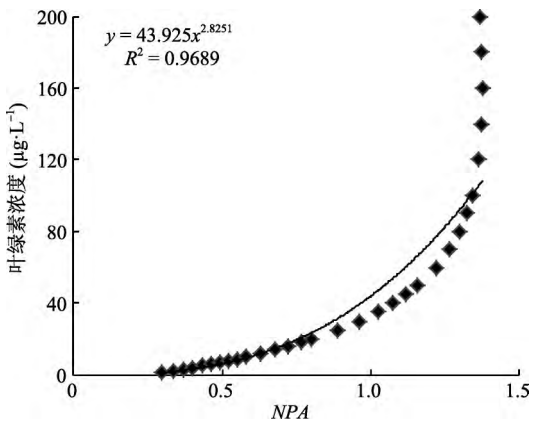

图3　叶绿素浓度与*NPA*的相关关系

Fig.3　Relationship between chlorophyll-a concentration and the *NPA*

3.3 其他常用反演模型

（1）红波段反射峰强度模型

由于叶绿素本身的结构和组成特性，使叶绿素在可见光的蓝和红波段有较强的吸收，而在绿波段有较强的反射。叶绿素在红波段670 nm处吸收最强，随着波长的增加，受叶绿素本身固有光学属性的影响，光谱反射率逐渐增加，在700 nm左右达到峰值，然后逐渐下降，但叶绿素在红光波段的反射强度比绿光波段的反射强度要低得多，在740 nm处表现出较强的吸收特性。在红光波段，随着叶绿素浓度的增加，反射峰强度逐渐增加，图5表明了叶绿素浓度同红光波段反射峰强度变化规律。

由图5可知，叶绿素在红波段的反射峰强度与浓度有较好的相关性，其决定系数为0.9604。利用叶绿素浓度与反射峰强度的相关关系反演叶绿素浓度，其RMS误差为3.69 μg·L⁻¹。

（2）红波段反射峰波长模型

在红波段区域，除反射峰强度受叶绿素浓度影响外，反射峰波长也随叶绿素浓度的增加逐渐向长波方向移动（图1）。反射峰波长随叶绿素浓度的变化规律可用线性函数关系来描述（图6）。利用反射峰波长同叶绿素浓度的函数关系反演叶绿素浓度，其决定系数为0.6513，RMS误差为33.04 μg·L⁻¹。

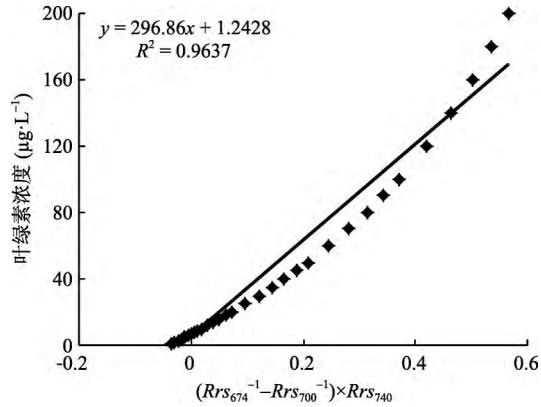

图4　叶绿素浓度和三波段模型[$(Rrs_{674}^{-1}-Rrs_{700}^{-1})\times Rrs_{740}$]的相关关系

Fig.4　Relationship between chlorophyll-a concentration and the three-band model

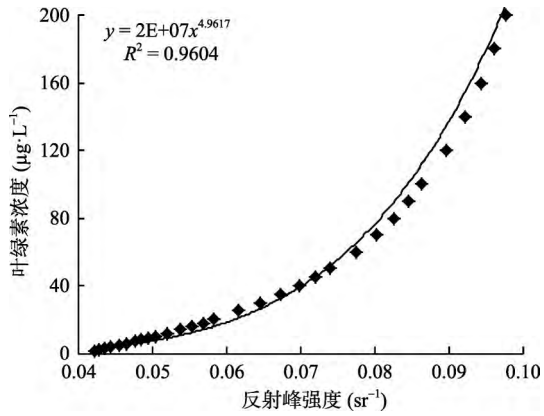

图5　叶绿素浓度随反射峰强度的变化规律

Fig.5　Relationship between chlorophyll-a concentration and the reflectance peak intensity in red band region

（3）红波段反射峰高度模型

叶绿素红波段反射峰高度（Red Line Height, RLH）（图7）依据叶绿素在红波段的光谱反射峰和相邻的2个吸收谷计算，类似于荧光线高度的计算[27-28]，公式为：

$$RLH = Rrs_{\max} - \frac{(740 - B_{\max})(Rrs_{674} - Rrs_{740})}{740 - 674} - Rrs_{740} \tag{6}$$

式（6）中，*RLH* 是叶绿素的红光线高度；Rrs_{λ} 是波长 λ 处的遥感反射率；$B_{\max}$ 是峰值波长。

通过研究红光线高度和叶绿素浓度的关系表

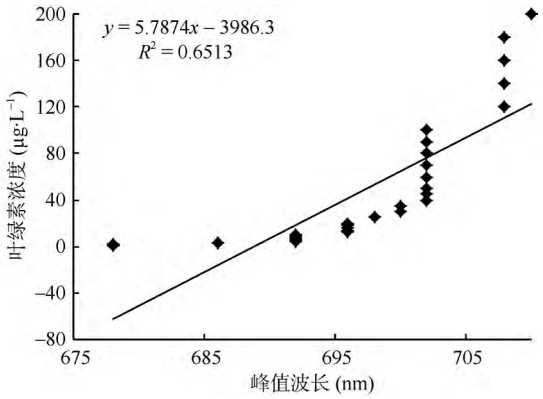

图6 叶绿素浓度随反射峰波长的变化规律

Fig.6 Relationship between chlorophyll-a concentration and the wavelength of reflectance peak

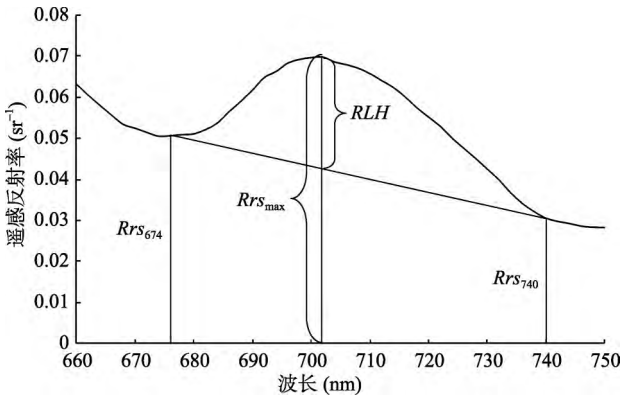

图7 红光线高度示意图

Fig.7 The illustration of the *RLH*

明，叶绿素浓度和红光线高度的决定系数为0.9711（图8），利用红光线高度模型反演叶绿素浓度其RMS误差为20.62 μg·L^{-1}。

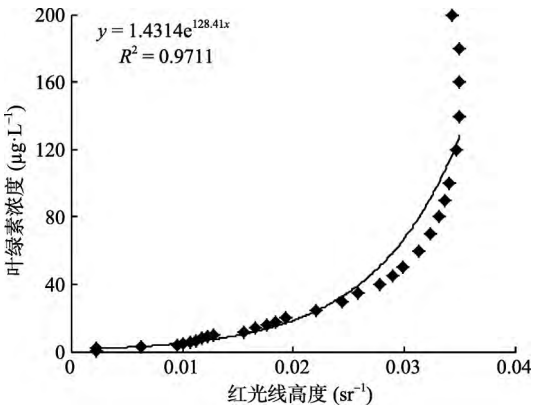

图8 叶绿素浓度和红光线高度的相关关系

Fig.8 Relationship between chlorophyll-a concentration and *RLH*

（4）比值模型

基于藻类叶绿素在红波段范围的吸收和光谱反射特性，除荧光峰算法外，叶绿素浓度的遥感反演中红波段比值算法是经常使用的方法。通过研究不同叶绿素浓度在红波段的反射峰与吸收谷比值同叶绿素浓度之间的关系表明，红波段比值同叶绿素浓度有较好的相关关系（R^2=0.9356）（图9）。利用比值算法对叶绿素浓度进行了反演，其RMS误差为10.67 μg·L^{-1}。

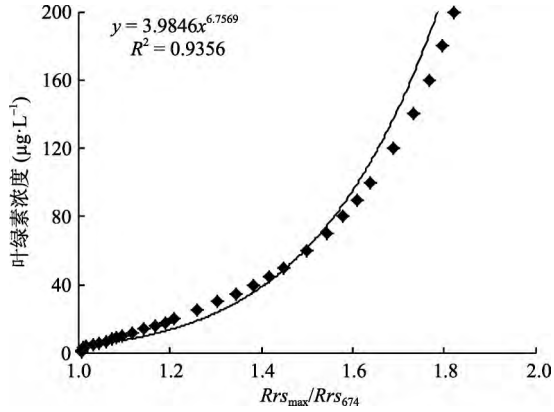

图9 叶绿素浓度同Rrs_{max}/Rrs_{674}的相关关系

Fig.9 Relationship between chlorophyll-a concentration and Rrs_{max}/Rrs_{674}

3.4 反演精度比较

通过对比叶绿素不同反演模型（表1），可知红光线高度模型和反射峰面积模型同叶绿素浓度决定系数最高，分别是0.9711和0.9689，其反演误差分别为20.62 μg·L^{-1}和25.25 μg·L^{-1}；其次是三波段模型和反射峰强度模型，决定系数分别为0.9637和0.9604，反演误差分别为10.66 μg·L^{-1}和3.69 μg·L^{-1}；比值模型反演精度也相对较高；反射峰波长模型反演精度最差。通过模拟数据对比研究叶绿素不同的反演模型可知，反射峰面积模型可以用来反演水

表1 水体叶绿素不同反演模型比较

Tab.1 Comparison between different chlorophyll-a retrieval models

反演模型	决定系数（R^2）	反演误差RMS（μg·L^{-1}）
反射峰面积模型	0.9689	25.25
三波段模型	0.9637	10.66
反射峰强度模型	0.9604	3.69
反射峰波长模型	0.6513	33.04
红光线高度模型	0.9711	20.62
比值模型	0.9356	10.67

体中叶绿素浓度，同其他常用模型相比而言，同样具有较高的反演精度。

4 结论

通过研究水体叶绿素反射光谱曲线，本文选取特征波段或波段组合建立了不同叶绿素浓度遥感反演模型。通过对模拟数据研究及不同反演模型对比分析，得出反射峰面积模型和叶绿素浓度相关性较好，其反演精度可以同其他经验模型进行比较。反射峰面积模型用来反演水体中叶绿素浓度，具有较高的决定系数。这主要是由于反射峰面积模型不仅考虑了水体中非色素悬浮物、黄色物质及水体后向散射对叶绿素浓度反演造成的影响，而且还综合考虑了叶绿素弹性散射效率的影响。基于Hydrolight模拟数据的研究结果表明，反射峰面积方法可用于现场实测高光谱数据来进行叶绿素浓度的遥感反演。

参考文献：

[1] O'Reilly J E, Maritorena S, Mitchell B G, *et al*. Ocean color chlorophyll algorithms for SeaWiFS[J]. Journal of Geophysical Research, 1998,103(C11):24937-24953.

[2] McClain C R, Feldman G C, Hooker S B. An overview of the SeaWiFS project and strategies for producing a climate research quality global ocean bio-optical time series [J]. Deep-Sea Research Part II, 2004,51(1-3):5-42.

[3] Stramski D, Bricaud A, Morel A. Modeling the inherent optical properties of the ocean based on the detailed composition of the planktonic community[J]. Applied Optics, 2001,40(18):2929-2945.

[4] Dall'Olmo G, Gitelson A A, Rundquist D C. Towards a unified approach for remote estimation of chlorophyll-a in both terrestrial vegetation and turbid productive waters [J]. Geophysical Research Letters, 2003,30(18):1938-1941.

[5] Gitelson A A, Schalles J F, Hladik C M. Remote chlorophyll-a retrieval in turbid, productive estuaries: Chesapeake Bay case study[J]. Remote Sensing of Environment, 2007,109(4):464-472.

[6] Gower J F R, Doerffer R, Borstad G A. Interpretation of the 685nm peak in water-leaving radiance spectra in terms of fluorescence, absorption and scattering, and its observation by MERIS[J]. International Journal of Remote Sensing, 1999,20(9):1771-1786.

[7] Vasilkov A, Kopelevich O. Reasons for the appearance of the maximum near 700 nm in the radiance spectrum emitted by the ocean layer[J]. Oceanology, 1982,22(5):697-701.

[8] Xing Q, Chen C, Shi H, *et al*. Estimation of chlorophyll-a concentrations in the Pearl River Estuary using in-situ hyperspectral data: A case study[J]. Marine Technology Society Journal, 2008,42(4):22-27.

[9] Stumpf R P, Tyler M A. Satellite detection of bloom and pigment distributions in estuaries[J]. Remote Sensing of Environment, 1988,24(3):358-404.

[10] Gons H J, Rijkeboer M, Ruddick K G. A chlorophyll-retrieval algorithm for satellite imagery (Medium Resolution Imaging Spectrometer) of inland and coastal waters [J]. Journal of Plankton Research, 2002,24(9):947-951.

[11] Ruddick K G, Gons H J, Rijkeboer M, *et al*. Optical remote sensing of chlorophyll a in case 2 waters by use of an adaptive two-band algorithm with optimal error properties[J]. Applied Optics, 2001,40(21):3575-3585.

[12] Gitelson A A, Vina A, Ciganda V, *et al*. Remote estimation of canopy chlorophyll content in crops[J]. Geophysical Research Letters, 2005,32(8):403-406.

[13] Gitelson A.A, Vina A, Arkebauer T J, *et al*. Remote estimation of leaf area index and green leaf biomass in maize canopies[J]. Geophysical Research Letters, 2003,30(5): 1248-1251.

[14] Gitelson A A, Dall'Olmo G, Moses W, *et al*. A simple semi-analytical model for remote estimation of chlorophyll-a in turbid waters: Validation[J]. Remote Sensing of Environment, 2008,112(9):3582-3593.

[15] Gitelson A, Keydan G, Shishkin V. Inland water quality assessment from satellite data in visible range of the spectrum[J]. Soviet Remote Sensing, 1985,6:28-36.

[16] Chen J, Zhang X, Quan W. Retrieval chlorophyll-a concentration from coastal waters: three-band semi-analytical algorithms comparison and development[J]. Optics Express, 2013,21(7):9024-9042.

[17] 马万栋,邢前国,张渊智,等.水体红波段反射光谱对叶绿素浓度变化的响应[J].光谱学与光谱分析,2010,30(2): 313-317.

[18] Gordon H R, Brown O B, Evans R H, *et al*. A semianalytic radiance model of ocean color[J]. Journal of Geophysical Research, 1988, 93(D9):10909-10924.

[19] Gordon H R, Brown O B, Jacobs M M. Computed relationships between the inherent and apparent optical properties of a flat homogeneous ocean[J]. Applied Optics, 1975,14(2):417-427.

[20] Morel A, Gentili B. Diffuse reflectance of oceanic waters. II. Bidirectional aspects[J]. Applied Optics, 1993, 32(33): 6864-6864.

[21] Garver S A, Siegel D A. Inherent optical property inversion of ocean color spectra and its biogeochemical interpretation. 1. Time series from the Sargasso Sea[J]. Journal of Geophysical Research, 1997,102(C2):18607-18625.

[22] Zaneveld J R V, Twardowski M J, Barbard A, *et al*. Intro-

duction to radiative transfer. Remote Sensing of Coastal Aquatic Environments[M]. Dordrecht: Springer, 2005.

[23] Zaneveld J R, Barnard A, Boss E. Theoretical derivation of the depth average of remotely sensed optical parameters[J]. Optics Express, 2005,13(22):9052-9061.

[24] Aas E, Højerslev N K. Analysis of underwater radiance observations: Apparent optical properties and analytic functions describing the angular radiance distribution[J]. Journal of Geophysical Research, 1999,104(C4):8015-8024.

[25] Devred E, Fuentes-Yaco C, Sathyendranath S, *et al*. A semi-analytic seasonal algorithm to retrieve chlorophyll-a concentration in the Northwest Atlantic Ocean from Sea WiFS data[J]. Indian Journal of Marine Science, 2005,34 (4):356-367.

[26] Ma W, Xing Q, Chen C, *et al*. Using the normalized peak area of remote sensing reflectance in the near-infrared region to estimate total suspended matter[J]. International Journal of Remote Sensing, 2011,32(22):7479-7486.

[27] Gower J, King S. Validation of chlorophyll fluorescence derived from MERIS on the west coast of Canada[J]. International Journal of Remote Sensing, 2007,28(3-4):625-635.

[28] Zhao D, Zhang F, Yang J, *et al*. The optimized spectral bands ratio for the relation of sun-induced chlorophyll fluorescence height with high chlorophyll a concentration of algal bloom waters[J]. Acta Oceanologica Sinica, 2005,27 (6):146-153.

Research on Chlorophyll-a Retrieval Simulation in Waters Based on the Normalized Peak Area

MA Wandong[1*], WANG Qiao[1], WU Chuanqing[1], YIN Shoujing[1], XING Qianguo[2], ZHU Li[1] and WU Di[1]

(1. *Satellite Environment Center, Ministry of Environmental Protection, Beijing* 100094, *China*; 2. *Yantai Institute of Coastal Zone Research, Chinese Academy of Sciences, Yantai* 264003, *China*)

Abstract: The chlorophyll-a concentration of waters is one of the main retrieval parameters in the field of water color remote sensing. Based on the coefficients of absorption and backscattering of waters, Colored Dissolved Organic Matter(CDOM), tripton and chlorophyll-a, which are achieved using the Hydrolight software package, the remote sensing reflectance is simulated according to the forward radiation transfer models without the consideration of fluorescence peak. And then, the spectral curves of variable chlorophyll-a concentration are achieved. The spectral characteristics of chlorophyll-a are analyzed according to these remote sensing reflectance curves. Next, the retrieval models of chlorophyll-a are built based on analyzing the spectral characteristics within selected bands or certain band combinations. In this paper, the Normalized Peak Area (NPA) model and three-band model are analyzed and applied to retrieve the chlorophyll-a concentration. As a comparison, other retrieval models are also considered. According to the analysis and results, we find that the chlorophyll-a concentration could be better retrieved by the NPA model, the three-band model, and a few other models, except for the model of reflectance peak position. The least competent retrieval model for chlorophyll-a is the model of reflectance peak position with the R^2 of 0.6513. Among all the retrieval models, the NPA model is the best model to retrieve cholorophyll-a concentration with the R^2 of 0.9689 and the RMS error of 25.25μg·L^{-1}. The second one is the three-band model with the R^2 of 0.9637 and the RMS error of 10.66μg·L^{-1}. The small retrieval error of the three-band model is due to the consideration of the backscattering impacts of tripton, CDOM and waters. The NPA model, in addition, has not only take into consideration of the backscattering impacts, but also the fluorescence efficiency and a variety of environmental factors when applied to retrieve chlorophyll-a concentration. In the end, we could conclude that the NPA could be utilized to retrieve chlorophyll-a concentration for simulated data. This conclusion should be further verified by using it with in situ experiments data.

Key words: chlorophyll-a; retrieval of remote sensing; the Normalized Peak Area model; the three-band model

***Corresponding author:** MA Wandong, E-mail：mawdcn@sohu.com